In Vivo Visualization of Amyloid Deposits in the Heart with ^{11}C-PIB and PET

Gunnar Antoni[1,2], Mark Lubberink[2,3], Sergio Estrada[1], Jan Axelsson[4], Kristina Carlson[5], Lars Lindsjö[2], Tanja Kero[2,3], Bengt Långström[6–8], Sven-Olof Granstam[9], Sara Rosengren[5], Ola Vedin[9], Cecilia Wassberg[2,3], Gerhard Wikström[9], Per Westermark[10], and Jens Sörensen[2,3]

[1]Platform for Preclinical PET, Department of Medicinal Chemistry, Uppsala University, Uppsala, Sweden; [2]PET Centre, Uppsala University Hospital, Uppsala, Sweden; [3]Nuclear Medicine and PET, Department of Radiology, Oncology and Radiation Sciences, Uppsala University, Uppsala, Sweden; [4]Radiation Physics, Department of Radiation Sciences, Umeå University, Umeå, Sweden; [5]Department of Hematology, Uppsala University Hospital, Uppsala, Sweden; [6]Department of Biochemistry and Organic Chemistry, Uppsala University, Uppsala, Sweden; [7]Neuropsychopharmacology Unit, Centre for Pharmacology and Therapeutics, Division of Experimental Medicine, Imperial College, London, United Kingdom; [8]PET and Cyclotron Unit, Department of Nuclear Medicine, Institute of Clinical Research, Odense University Hospital, University of Southern Denmark, Odense, Denmark; [9]Department of Medical Sciences, Uppsala University, Uppsala, Sweden; and [10]Department of Immunology, Genetics and Pathology, Uppsala University, Uppsala, Sweden

Cardiac amyloidosis is a differential diagnosis in heart failure and is associated with high mortality. There is currently no noninvasive imaging test available for specific diagnosis. *N*-[*methyl*-^{11}C]2-(4′-methylamino-phenyl)-6-hydroxybenzothiazole (^{11}C-PIB) PET is used in the evaluation of brain amyloidosis. We evaluated the potential use of ^{11}C-PIB PET in systemic amyloidosis affecting the heart. **Methods:** Patients (n = 10) diagnosed with systemic amyloidosis—including heart involvement of either monoclonal immunoglobulin light-chain (AL) or transthyretin (ATTR) type—and healthy volunteers (n = 5) were investigated with PET/CT using ^{11}C-PIB to study cardiac amyloid deposits and with ^{11}C-acetate to measure myocardial blood flow to study the impact of global and regional perfusion on PIB retention. **Results:** Myocardial ^{11}C-PIB uptake was visually evident in all patients 15–25 min after injection and was not seen in any volunteer. A significant difference in ^{11}C-PIB retention in the heart between patients and healthy controls was found. The data indicate that myocardial amyloid deposits in patients diagnosed with systemic amyloidosis could be visualized with ^{11}C-PIB. No correlation between ^{11}C-PIB retention index and myocardial blood flow as measured with ^{11}C-acetate was found on the global level, whereas a positive correlation on the segmental level was seen in a single patient. **Conclusion:** ^{11}C-PIB and PET could be a method to study systemic amyloidosis of type AL and ATTR affecting the heart and should be investigated further both as a diagnostic tool and as a noninvasive method for treatment follow-up.

Key Words: amyloid; PET imaging; ^{11}C-PIB; ^{11}C-acetate; amyloid; transthyretin; systemic amyloidosis; myocardial blood flow

J Nucl Med 2013; 54:213–220
DOI: 10.2967/jnumed.111.102053

Received Dec. 17, 2011; revision accepted Aug. 29, 2012.
For correspondence or reprints contact either of the following:
Gunnar Antoni, PET Centre, Uppsala University Hospital, SE-751 85 Uppsala, Sweden.
E-mail: Gunnar.Antoni@akademiska.se
Per Westermark, Rudbeck Laboratory, SE-751 85 Uppsala, Sweden.
E-mail: per.westermark@igp.uu.se
Published online Dec. 13, 2012

Amyloids are highly organized aggregates rich in cross β-sheet proteins that are found, for example, in Alzheimer's disease and systemic amyloidosis (*1*). The diseases are characterized by a variety of normal or mutated proteins that are deposited extracellularly and disrupt organ function either mechanically or by exerting direct toxic effects on cells (*2*). All organs except for the brain can be affected in systemic amyloidosis, and the disease is often life-threatening. A biopsy from a symptom-giving organ or from a tissue that regularly contains amyloid provides the diagnosis. Presently, a subcutaneous adipose tissue biopsy is often used, and the biopsy sample also determines the biochemical type (*3*). Heart involvement, leading to cardiac insufficiency or to arrhythmias, is one of the most important and life-threatening manifestations in several of the systemic amyloidoses, particularly of immunoglobulin light-chain (AL) and transthyretin (ATTR) type.

Early diagnosis before structural change to heart tissue has occurred is important both for the disease prognosis and for the monitoring of treatment effects. The assessment of cardiac amyloidosis includes a number of diagnostic methods, but there is no method available for direct visualization and quantification of the amyloid deposits in the heart. Echocardiography is the mainstay of imaging in cardiac amyloidosis. Both the systolic and diastolic component of heart failure can be assessed using a combination of traditional techniques such as 2-dimensional Doppler and tissue Doppler. Even in clear cases, findings are difficult to differentiate from other types of concentric hypertrophy, but the combination of typical findings and a positive biopsy result from any organ is regarded as evidence of cardiac involvement. A variety of newer echocardiography techniques is under investigation and might improve the accuracy (*4*).

Additionally, MR imaging with gadolinium-based contrast medium and late enhancement in T1-weighted images provides a method by which the location and extent of extracellular infiltration of amyloid deposits can be visualized (*5*), but this technique is not specific for amyloidosis on the molecular level.

Several molecular imaging methods that depend on the binding of specific ligands to amyloid are available. Serum amyloid P is a ubiquitous component of in vivo amyloid and binds avidly to cross β-sheet fibrils. ^{123}I-serum amyloid P scanning has come to be a valuable and specific method to visualize the distribution of amyloid in the body (*6,7*). By this method, it is also possible to follow the resolution of amyloid, particularly in serum amyloid A and amyloid amyloidosis. However, the heart is not visualized by ^{123}I-serum amyloid P scanning (*7*). ^{123}I-meta-iodobenzylguanidine has shown the most clinical relevance, and a correlation between reduced tracer accumulation in the myocardium and impaired cardiac sympathetic innervation has been found (*8*). This correlation is, however, not evidence for or a measure of amyloid deposits. The polypeptide protease inhibitor aprotinin (*9,10*) has been labeled with ^{99m}Tc and used for visualization of amyloid deposits in the myocardium, with antiproteases, found in amyloid deposits, as the suggested molecular target. In addition, ^{99m}Tc-DPD is used as an imaging agent for the visualization of transthyretin-related amyloidosis (*11*). However, with SPECT, no quantification of the radioactivity in tissue can be obtained, and another diagnostic imaging modality is required to achieve quantitative measures of tracer binding to tissue. A light-chain monoclonal antibody, 11-1F4, has been labeled with ^{124}I and used in PET studies on patients diagnosed with amyloid amyloidosis. Uptake was found in some organs with amyloid deposits, for example, the liver, but not in heart or kidneys (*12*). The PET tracer *N*-[*methyl*-^{11}C]2-(4′-methylamino-phenyl)-6-hydroxybenzothiazole (^{11}C-PIB) was developed for visualization and quantification of β-amyloid in Alzheimer's disease and is believed to bind to amyloid fibrils of any type (*13*). However, this tracer has not yet been evaluated for use with cardiac amyloidosis.

The aim of the present work was to investigate whether amyloid deposits in the heart can be visualized and quantified noninvasively in patients diagnosed with systemic amyloidosis by comparison with healthy age-matched controls using ^{11}C-PIB and PET. The relationship between ^{11}C-PIB uptake and myocardial blood flow (MBF), and the possible dependence of ^{11}C-PIB uptake on MBF, was assessed using ^{11}C-acetate PET.

MATERIALS AND METHODS

Subjects

Ten patients (mean age, 66 y; age range, 48–77 y) and 5 healthy controls (mean age, 64 y; age range, 54–75 y) participated in this study. The age-matched controls were healthy as assessed by medical history. Each volunteer provided written informed consent. The study was performed with permission from the local Independent Ethics Committee and Radiation Protection Committee and in accordance with the International Conference on Harmonisation Good Clinical Practice Guidelines and the Declaration of Helsinki. Patients were included on the basis of immunohistochemistry-confirmed amyloid disease in subcutaneous tissue samples, and heart involvement was diagnosed either by echocardiography ($n = 10$) or by myocardial biopsy ($n = 5$), according to the criteria published by Gertz et al. (*14*).

The nature of the amyloid was determined in all patients either by immunohistochemistry or by Western blot analysis. For immunohistochemistry, endomyocardial biopsy samples were incubated with the polyclonal rabbit antiserum 1898 against recombinant TTR50-127 developed in-house (*15*), the monoclonal antibody pwlam against AL λ (*16*), and the monoclonal antibody Sne5 against protein serum amyloid A (unpublished data, Nyström and Westermark). Western blot analyses were performed on extracts from subcutaneous adipose tissue biopsies using antibodies as previously described (*17*).

PET/CT Procedure

After low-dose CT scanning, a 32-min dynamic emission scan of the heart was started simultaneously with the intravenous bolus injection of ^{11}C-acetate (10 MBq/kg) using a Discovery ST PET/CT scanner (GE Healthcare). After at least 2 h to allow for the decay of remaining activity, a second low-dose CT scan was made, followed by a second 25-min dynamic scan starting simultaneously with intravenous bolus injection of ^{11}C-PIB (6 MBq/kg). Imaging was performed in 2-dimensional mode, yielding 47 transaxial images. All appropriate corrections for scanner normalization, dead time, decay, scatter, randoms, and attenuation were applied. Images were reconstructed into 32 frames (^{11}C-acetate; 12×5, 6×10, 4×30, 4×60, 2×120, and 4×300 s) or 29 frames (^{11}C-PIB; 12×5, 6×10, 4×30, 2×60, 2×120, and 3×300 s) using ordered-subset expectation maximization (2 iterations, 30 subsets), with the application of a 5-mm Gaussian filter. Images consisted of 128×128 voxels, with dimensions of $2.34 \times 2.34 \times 3.27$ mm and a spatial resolution of approximately 7 mm.

Image Analysis

^{11}C-Acetate MBF Images. Using the CAPP package (Siemens/CTI), we placed 1-cm-diameter regions of interest over the ascending aorta in 10 consecutive image planes of the frame in which the first pass of ^{11}C-acetate could best be seen, and then regions of interest were combined into a volume of interest (VOI). A second VOI was placed over the right ventricular cavity, with boundaries at a minimum of 1 cm from its wall. VOIs were transferred to all image frames to create arterial and right-ventricular time–activity curves $C_A(t)$ and $C_{RV}(t)$, respectively. An image-derived input function $C_P(t)$ was created by multiplying $C_A(t)$ by a sigmoid function fit to published population-averaged metabolite data (*18–20*). Parametric K_1 (influx rate constant of ^{11}C-acetate) images were calculated using a basis-function implementation (*21–23*) of the solution of a single-tissue-compartment model with corrections for blood volume and left-ventricular (LV) and right-ventricular spillover, as suggested by Van den Hoff et al. (*20*):

$$C_{PET} = (1 - V_A - V_{RV}) \times K_1 \times C_P(t) \otimes e^{-k_2 t} + V_A C_A(t) + V_{RV} C_{RV}(t). \quad \text{Eq. 1}$$

Here, V_A accounts for LV spill-over and arterial blood volume, V_{RV} is right-ventricular spill-over, and k_2 is the efflux rate constant of ^{11}C-acetate. Thirty logarithmically spaced precomputed basis functions $f_i(t)$ were used, with k_2 values ranging from 0.05 to

0.2 min^{-1}. K_1 images were converted to MBF images using the relationship reported by Van den Hoff et al. (*19,20*).

^{11}C-PIB. An ^{11}C-PIB arterial time–activity curve was calculated in the same manner as described for ^{11}C-acetate. ^{11}C-PIB sum images (15–60 s after injection) were coregistered to the ^{11}C-acetate sum images (15–60 s after injection), both mainly showing blood volume, using rigid mutual information registration as implemented in the Voiager software package (GE Healthcare). Using the same transformation, we then coregistered the full dynamic PIB scan to the ^{11}C-acetate scan.

Region-of-Interest Analysis. ^{11}C-acetate MBF images were transformed to short-axis images using the CAPP package, and the same transformation was applied to the coregistered ^{11}C-PIB images. A single VOI was drawn over the entire left myocardial wall in apical, mid, and basal planes on the short-axis MBF images, giving the mean MBF of the whole myocardium excluding apex, and transferred to ^{11}C-PIB images. Additionally, the left myocardial wall was divided into 16 standardized segments according to the definition of the American Heart Association, excluding apex (*24*). The ^{11}C-PIB retention index (RI) was calculated as the mean ^{11}C-PIB radioactivity concentration between 15 and 25 min after injection divided by the integral of the arterial time–activity curve between 0 and 20 min after injection, the mid time of the 15- to 25-min interval. Differences in whole myocardium ^{11}C-PIB RI and MBF between patients and healthy controls were assessed using Mann–Whitney *U* tests. Correlation between MBF and RI was assessed using the Pearson correlation coefficient for both global and segmental values.

In Vitro Binding Studies

A Kinematica polytron was used to homogenize postmortem samples of tissue from 1 patient heart and 3 control hearts on ice in 50 volumes of 0.3 M sucrose, and the samples were then stored at −80°C until use. Heart samples were collected from 4 regions from a patient with systemic amyloidosis of transthyretin type who had participated in the clinical PET study. Cardiac tissue from 3 control individuals was acquired from a donated sample collection. The individuals had died from various diseases, but the tissue was previously shown to be void of amyloid. For the binding assay, homogenates were thawed and 5-μL aliquots were incubated at room temperature for 40 min with ^{11}C-PIB at a final concentration of 5 nM in phosphate-buffered saline (pH 7.4) containing 0.5% bovine serum albumin, in a total volume of 1 mL. Triplicate samples were used. Nonspecific binding was defined as the residual binding in the presence of 5 μM unlabeled PIB. Specific ^{11}C-PIB binding to patient heart homogenates was compared with that in control hearts.

Statistical Analysis

Measurements are presented as mean and range unless otherwise stated. A Mann–Whitney *U* test was used to assess differences between patients and healthy controls. Correlations were evaluated using Pearson coefficient tests. A 2-sided *P* value of less than 0.05 was considered significant.

RESULTS

Clinical Data

The patient group consisted of 5 individuals who had received melphalan for 6–54 mo before the PET investigation and 5 who had received no antiamyloid medications. Table 1 summarizes patient and healthy volunteer data. The diagnosis of cardiac amyloidosis was established by myocardial biopsy ($n = 5$) or by a positive biopsy result from subcutaneous abdominal fat in combination with typical findings on echocardiography.

Echocardiography data were acquired in all patients for clinical reasons within 206 ± 149 d of PET. In 2 patients, pre-PET echocardiography was of poor quality or not retrievable and therefore echocardiography was repeated after PET. Overall, the echocardiography findings were characterized as typical for patients with cardiac amyloidosis with normal or mildly decreased LV ejection fraction (0.53 [range, 0.42–0.66]), concentric LV hypertrophy and signs of a diastolic dysfunction with increased left atrial size, and Doppler findings such as restrictive diastolic dysfunction. Mean LV wall thickness in diastole was 1.7 cm (range, 1.3–2.2 cm) in the interventricular septum and 1.6 cm (range, 1.3–2.1 cm) in the posterior wall. Mean right-ventricular wall thickness was 0.6 cm (range, 0.5–1.2 cm). All patients had at least some electrocardiogram (ECG) signs of LV pathology but a low-voltage electrocardiogram was noted in only 3 of 10. Eight of 10 patients had Q-waves, which were interpreted as pseudoinfarction due to amyloid burden in 6 patients and as a true infarction in 2 patients with a documented history of concomitant ischemic heart disease. Four patients had chronic atrial fibrillation, whereas the remaining 6 had sinus rhythm.

Mean time–activity curves for ^{11}C-PIB in blood and myocardium are shown in Figure 1 (normalized injected activity [standardized uptake value] divided by body weight). Individual time–activity curves are shown in Supplemental Figure 1 (supplemental materials are available online only at http://jnm.snmjournals.org). Figure 2 shows representative MBF and ^{11}C-PIB RI images from 1 healthy volunteer and 3 patients. Visual inspection of ^{11}C-PIB summation images acquired at 15–25 min after injection showed obvious uptake in the LV wall of all patients, whereas no uptake was seen in any of the 5 healthy controls (Fig. 2). In half of the patients, ^{11}C-PIB uptake was visually detectable also in the right ventricular wall. Nine of the patients had signs of reversible uptake, with a maximum concentration at around 10–15 min after injection.

The mean ^{11}C-PIB RI in amyloidosis patients was 0.054 min^{-1} (range, 0.033–0.134 min^{-1}), compared with 0.025 min^{-1} (range, 0.020–0.031 min^{-1}) in healthy controls. Mean MBF as measured by ^{11}C-acetate was 0.49 mL cm^{-3} min^{-1} (range, 0.28–0.69 mL cm^{-3} min^{-1}) in patients and 0.71 mL cm^{-3} min^{-1} (range, 0.52–1.07 mL cm^{-3} min^{-1}) in controls. As shown in Figure 3, there was a significant difference in the ^{11}C-PIB RI between amyloidosis patients and healthy controls ($P = 0.0007$). In addition, MBF was significantly lower in amyloidosis patients ($P = 0.03$). Blood flow–corrected RI (RI/MBF) was also significantly higher in amyloidosis patients, at 0.124 (range, 0.069–0.309), than in healthy controls, at 0.042 (range, 0.025–0.052) ($P = 0.0007$).

No significant correlation between MBF and RI was found on the global level as indicated in Figure 4, either for controls and patients together (Pearson correlation coefficient

TABLE 1
Patient and Healthy Control Data

Subject	Sex	Age (y)	Ischemic heart disease	Diagnosis	Melphalan*	IVSd† (cm)	Posterior wall thickness (cm)	RV‡ (cm)	E/e§	LV ejection fraction	LV end-diastolic volume (mL)	Left atrial volume (mL m^{-2})	RI for ^{11}C-PIB (min^{-1})	MBF (mL cm^{-3} min^{-1})
1	M	55	No	Transthyretin‖	No	1.7	1.7	0.8	17	0.54	83	34	0.071	0.59
2	F	63	Yes	AL κ	Yes	1.6	1.3	0.5	22	0.56	46	41	0.075	0.72
3	M	71	No	Transthyretin¶	No	2.0	1.6	0.7	15	0.43	75	40	0.033	0.24
4	M	63	No	AL λ	Yes	1.9	1.6	0.5	—	0.44	152	45	0.036	0.33
5	M	75	Yes	AL λ	No	1.7	1.6	0.5	10	0.42	82	74	0.048	0.52
6	M	48	No	AL λ	Yes	1.8	1.7	0.7	11	0.66	98	38	0.042	0.54
7	M	67	No	AL κ	Yes	1.3	1.5	0.4	21	0.67	84	56	0.039	0.47
8	M	65	No	Transthyretin‡	No	2.2	2.1	1.2	29	0.48	58	33	0.033	0.34
9	M	76	No	AL λ	No	1.5	1.4	0.7	20	0.42	80	48	0.134	0.46
10	M	77	No	AL λ	Yes	1.5	1.5	0.6	—	0.64	95	52	0.033	0.52
11	M	75	No	Healthy	No								0.020	0.60
12	F	71	No	Healthy	No								0.023	1.08
13	M	60	No	Healthy	No								0.029	0.63
14	M	61	No	Healthy	No								0.031	0.74
15	F	54	No	Healthy	No								0.023	0.52

*Antiamyloid treatment before PET.
†Interventricular septal wall thickness in diastole.
‡Thickness of right ventricular free wall.
§Ratio of E-wave deceleration time and septal wall motion at time of early mitral flow.
‖Familial Val30Met transthyretin.
¶Senile systemic amyloidosis.

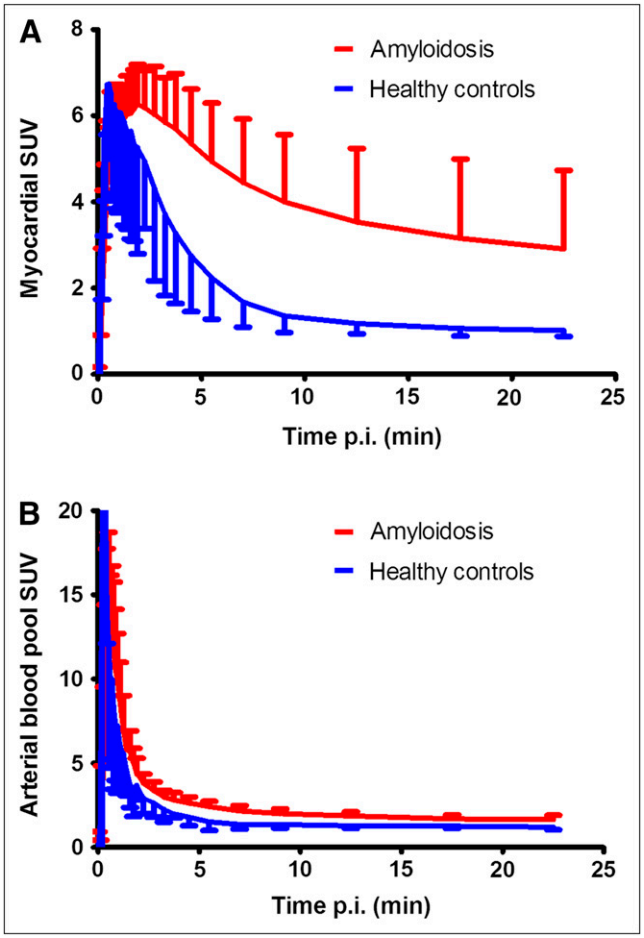

FIGURE 1. Mean standardized uptake value vs. time curves of ^{11}C-PIB in whole myocardium (A) and arterial blood (B) for amyloidosis patients (red) and healthy controls (blue). Error bars represent 95% confidence intervals. p.i. = after injection; SUV = standardized uptake value.

$r^2 = 0.01$, $P = 0.67$) or separately (patients: $r^2 = 0.13$, $P = 0.30$; controls: $r^2 = 0.01$, $P = 0.95$). Similarly, there was no significant correlation between MBF and RI on the segmental level for absolute values or when segmental values were normalized to the segment with the highest value of either. With an intraindividual analysis on the segment level, the patient with the highest RI (patient 9) had a highly significant positive correlation between MBF and RI ($r^2 = 0.85$, $P < 0.001$), whereas no such pattern was found for any other patient or healthy control.

^{11}C-PIB In Vitro Binding: Postmortem Case

The binding of ^{11}C-PIB to postmortem heart tissue (from patient 3) and normal heart homogenates was determined by radioligand assay using ^{11}C-PIB at 5 nM. In the 4 samples from 1 heart with transthyretin, the average amount of specifically bound ^{11}C-PIB was 2.0 ± 0.5 pmol/mg. This average was significantly higher than the average uptake in the 3 control hearts, which was 0.06 ± 0.04 pmol/mg of wet tissue (Fig. 5).

DISCUSSION

^{11}C-PIB is believed to bind with conformational dependence to amyloid fibrils of any type—a belief that is in agreement with the results of the present study. The in vitro tissue analysis that was performed in the present study confirmed that there was specific binding of ^{11}C-PIB in heart tissue with amyloid deposits. Amyloid deposits in the myocardium of patients diagnosed with systemic amyloidosis of AL κ, AL λ, and transthyretin origin could be visualized with ^{11}C-PIB, and patients could be identified by visual and semiquantitative assessment of ^{11}C-PIB RI images. In patients with amyloidosis, a significant increase in the ^{11}C-PIB RI was found, whereas MBF was significantly reduced. Obviously, increased ^{11}C-PIB retention was not due to increased MBF. In most patients, ^{11}C-PIB uptake in the myocardium was rather homogeneous, as was MBF. In a single patient (patient 5 in Fig. 2), however, increased ^{11}C-PIB RI was mainly confined to the septum, which showed a corresponding perfusion defect. Although no significant correlation between ^{11}C-PIB RI and MBF was found (Fig. 4), possibly because of the small patient group and large normal interindividual

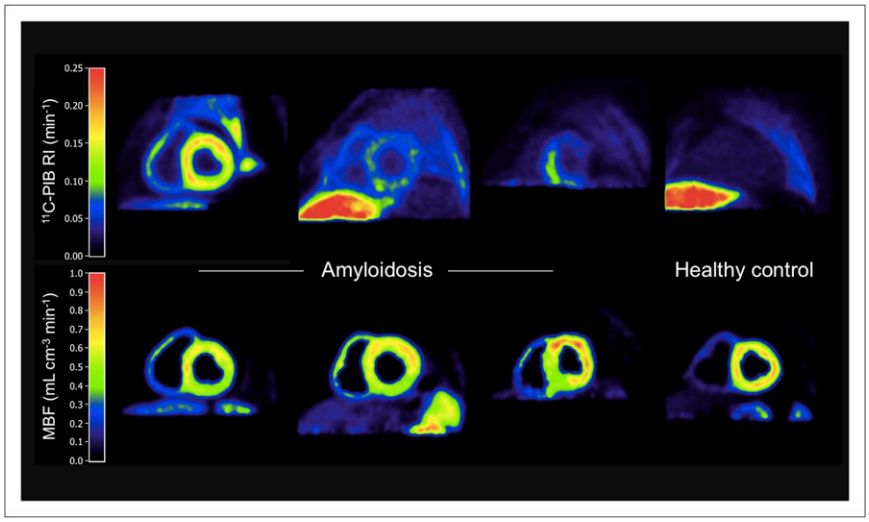

FIGURE 2. Short-axis images of ^{11}C-PIB RI and MBF in (left to right) patients with high (patient 9 in Table 1), intermediate (patient 1), and partially increased (patient 5) ^{11}C-PIB retention and a healthy control. Liver is clearly visible in^{11}C-PIB images of patient 1 and healthy control and is just outside PET field of view for other 2 patients. Liver uptake is due to biliary excretion of ^{11}C-PIB and is likely not related to amyloid binding.

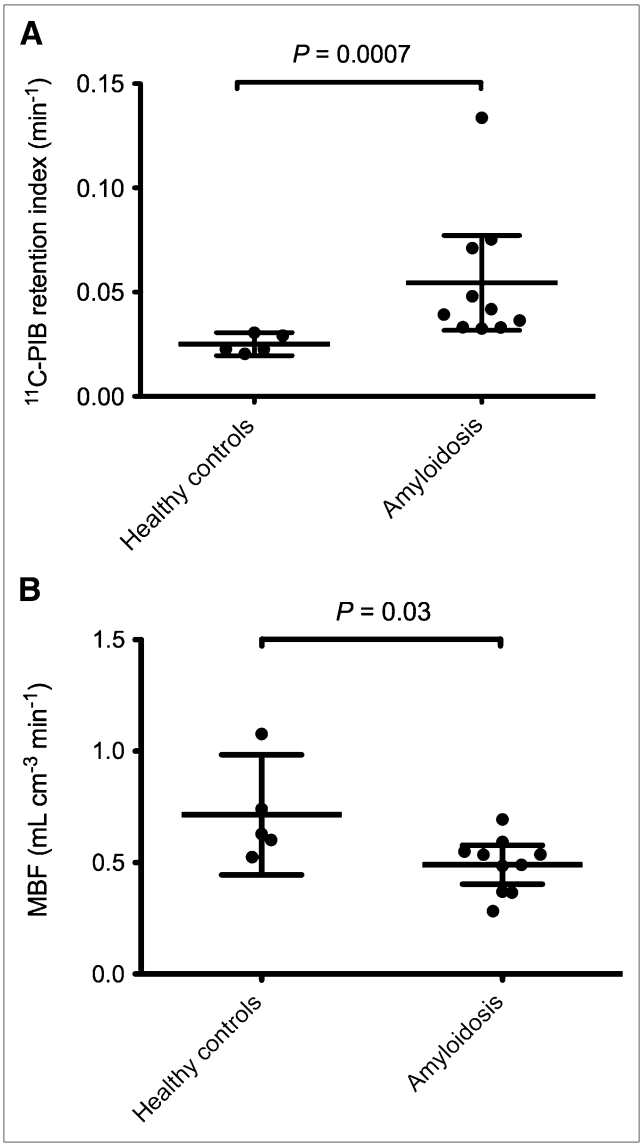

FIGURE 3. ^{11}C-PIB RI (A) and MBF (B) in healthy controls and amyloidosis patients. Horizontal lines indicate mean and 95% confidence intervals.

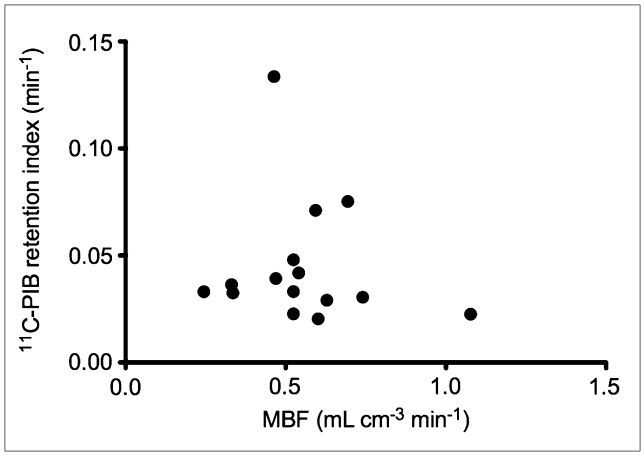

FIGURE 4. ^{11}C-PIB RI vs. MBF in all amyloidosis patients and healthy controls.

differences in resting-state MBF values, these results do suggest that increased ^{11}C-PIB is associated with a decrease in MBF. In a single patient (patient 9), there was a strong positive correlation between ^{11}C-PIB RI and MBF on a segmental level, not seen in any other patient or any healthy control. This particular patient had the highest ^{11}C-PIB RI, and the time–activity curves indicated minimal reversibility of ^{11}C-PIB binding during the 25 min of scanning. Specifically, this correlation was not present in any other patient with an AL λ amyloid type, which seems to indicate that the molecular mechanisms of PIB binding are heterogeneous even for the same amyloid type and that perfusion measurements might be needed also in future quantitative studies to account for variable PIB delivery to tissue in some cases.

There was a significantly larger ^{11}C-PIB RI in the patients with known amyloidosis than in healthy volunteers. This finding is encouraging in terms of establishing an objective method in a clinical routine, to document cardiac amyloidosis in patients for whom cardiac biopsy material is not available. However, the number of subjects in this study was small and did not include patients with diastolic heart failure without cardiac amyloidosis. Senile systemic amyloidosis (from wild-type transthyretin) with myocardial deposits is common in elderly subjects and is presently underdiagnosed and probably without symptoms at an early stage (*25*). It is possible that such amyloid deposits will be diagnosed by the use of PIB. Further studies negating ^{11}C-PIB uptake in heart failure patients without amyloidosis are needed before the method is implemented in a routine setting.

Semiquantitative assessment of ^{11}C-PIB binding by RI takes into account interindividual variations in blood clearance without the need for blood sampling and thus is feasible for routine clinical use. However, the use of RI disregards interindividual differences in plasma metabolism and plasma–free fractions and the consequent differences that may exist in the actual amount of nonmetabolized ^{11}C-PIB in plasma available for uptake in the myocardium. Previous studies with, for example, ^{11}C-hydroxyephedrine have shown that, for that tracer, RI correlated well with the actual volume of distribution (V_T) as determined by tracer kinetic modeling with a metabolite-corrected plasma input function, although the slope of the relation between RI and V_T decreased somewhat for higher V_T values (*26*). This correlation remains to be validated for ^{11}C-PIB and will be the subject of future studies. Furthermore, the optimal time point for assessment of RI, resulting in optimal discrimination between patients and controls, needs to be addressed. Figure 6 shows RI as a function of time. As is obvious from Figure 6, RI decreases with time. However, the ratio between RI values in patients and controls, after an initial increase with time, remains constant for time points after 10 min. As such, any chosen interval for the calculation of RI between 10 and 25 min after injection results in a full separation between patients and controls and would have given similar conclusions.

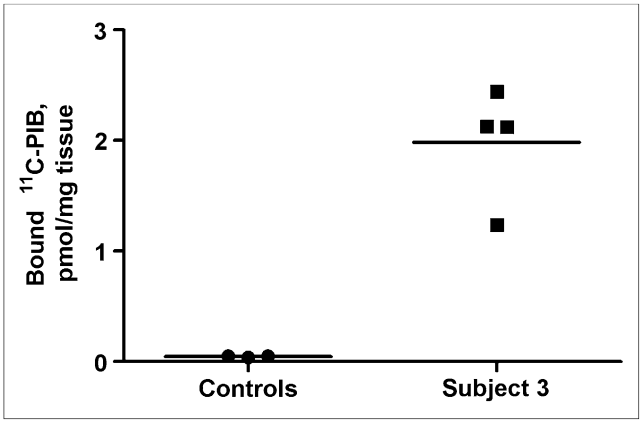

FIGURE 5. Specific binding of ^{11}C-PIB to homogenates from control hearts (n = 3) and from 4 regions (mean value shown) of heart with systemic amyloidosis (transthyretin).

Assuming that the healthy controls did not have any specific ^{11}C-PIB binding at all, a normal RI value should be close to zero at sufficiently long times after injection. RI calculations are much simpler than full compartmental analyses and could be feasible in a clinical environment, but the fact that these calculations do not differentiate specific binding to amyloid from nonspecific tracer uptake and tracer in the blood pool is the likely reason for the nonzero RI control values. Further studies should evaluate the compartment-analysis approach in this context and might also be needed for ^{11}C-PIB PET to rule out early cardiac amyloidosis.

In the present work, ^{11}C-acetate was used to measure MBF. Although previous studies have shown a good correlation between MBF based on ^{11}C-acetate and MBF as measured by ^{13}N-ammonia (*20*) and ^{15}O-water (*19*), both in healthy controls and patients with hypertrophic cardiomyopathy, the use of ^{11}C-acetate for MBF measurements in amyloidosis patients has not been validated. A possible explanation for the low apparent MBF in the patient group could be partial-volume effect. In later stages of systemic amyloidosis involving the heart, a significant part of the total enlarged myocardial mass consists of amyloid deposits. Amyloid deposits are the substrate both for diagnosis of increased wall thicknesses using echocardiography and for low-voltage amplitudes and Q-waves using electrocardiography. They are not scarred tissue but nonfunctional, probably nonperfusable, myocardium with a mechanical restriction, resulting in a reduced apparent transmural MBF as measured by ^{11}C-acetate, because the kinetic model measures the mean perfusion in both perfusable and nonperfusable tissue. It may well be the case that MBF is normal in remaining perfusable tissue, and future studies will include MBF measurements with ^{15}O-water, with which MBF measurements solely in perfusable tissue can be obtained as well (*27*).

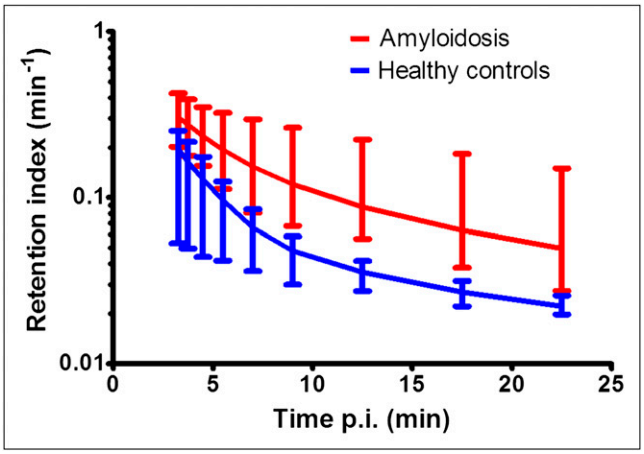

FIGURE 6. ^{11}C-PIB RI vs. time in amyloidosis patients (red) and healthy controls (blue). Error bars represent range of data. p.i. = after injection.

Eight of 10 patients in this study had Q-wave signs of pseudoinfarction according to electrocardiography, but only 2 patients had known ischemic heart disease with documented acute myocardial infarctions (one of whom was patient 5). Patient 5 had regionally increased ^{11}C-PIB and a perfusion defect in the septal wall, indicating coexistence of amyloid and infarction. This phenomenon supports a previous finding that regional amyloid burden can potentially induce ischemia and infarction even with morphologically normal angiograms (*28*).

One of the future aims of the current project is to investigate the potential of a quantitative PET–based method to assess amyloid burden and the dynamics of amyloid turnover in response to directed therapy. Of the 10 patients investigated, 5 had received melphalan treatment for 6–54 mo before the PET scan. No significant difference in ^{11}C-PIB RI was found between the groups of patients with and without treatment. A possible explanation, that the interindividual variation in ^{11}C-PIB retention is larger than the changes in ^{11}C-PIB retention caused by melphalan treatment, needs to be further investigated in future studies.

CONCLUSION

^{11}C-PIB can visualize amyloid deposits in the heart. Binding is variable and has some degree of reversibility, favoring an early time window for imaging. The mechanism of retention in the heart is unclear but does not appear to be positively related to myocardial perfusion in most cases. The use of ^{11}C-PIB with PET is a new noninvasive method to study systemic amyloidosis affecting the heart and may become a clinically feasible method for diagnosis and treatment follow-up.

DISCLOSURE

The costs of publication of this article were defrayed in part by the payment of page charges. Therefore, and solely to indicate this fact, this article is hereby marked "advertisement" in accordance with 18 USC section 1734. The study was financially supported by the Amersham Fund at Uppsala University, the Swedish Research Council, FAMY, FAMY Norrbotten and AMYL. No other potential conflict of interest relevant to this article was reported.

ACKNOWLEDGMENTS

We thank the staff at the PET Centre at Uppsala University Hospital for their assistance with the scans, and Dr. Lieuwe Appel for valuable discussions on the manuscript.

REFERENCES

1. Merlini G, Westermark P. The systemic amyloidoses: clearer understanding of the molecular mechanisms offers hope for more effective therapies. *J Intern Med.* 2004;255:159–178.
2. Sipe JD, Benson MD, Buxbaum JN, et al. Amyloid fibril protein nomenclature: 2010 recommendations from the nomenclature committee of the International Society of Amyloidosis. *Amyloid.* 2012;19:167–170.
3. Brambilla D, Souguir H, Nicolas J, et al. Colloidal properties of biodegradable nanoparticles influence interaction with amyloid-beta peptide. *J Biotechnol.* 2010;156:338–340.
4. Liu D, Niemann M, Hu K, et al. Echocardiographic evaluation of systolic and diastolic function in patients with cardiac amyloidosis. *Am J Cardiol.* 2011;108: 591–598.
5. Syed IS, Glockner JF, Feng D, et al. Role of cardiac magnetic resonance imaging in the detection of cardiac amyloidosis. *JACC Cardiovasc Imaging.* 2010;3:155–164.
6. Hawkins PN, Richardson S, Vigushin DM, et al. Serum amyloid P component scintigraphy and turnover studies for diagnosis and quantitative monitoring of AA amyloidosis in juvenile rheumatoid arthritis. *Arthritis Rheum.* 1993;36:842–851.
7. Hazenberg BP, van Rijswijk MH, Piers DA, et al. Diagnostic performance of ^{123}I-labeled serum amyloid P component scintigraphy in patients with amyloidosis. *Am J Med.* 2006;119:355 e315-324.
8. Knuuti J, Sipola P. Is it time for cardiac innervation imaging? *Q J Nucl Med Mol Imaging.* 2005;49:97–105.
9. Aprile C, Marinone G, Saponaro R, Bonino C, Merlini G. Cardiac and pleuropulmonary AL amyloid imaging with technetium-99m labelled aprotinin. *Eur J Nucl Med.* 1995;22:1393–1401.
10. Han S, Chong V, Murray T, et al. Preliminary experience of ^{99m}Tc-aprotinin scintigraphy in amyloidosis. *Eur J Haematol.* 2007;79:494–500.
11. Puille M, Altland K, Linke RP, et al. ^{99m}Tc-DPD scintigraphy in transthyretin-related familial amyloidotic polyneuropathy. *Eur J Nucl Med Mol Imaging.* 2002;29:376–379.
12. Wall JS, Kennel SJ, Stuckey AC, et al. Radioimmunodetection of amyloid deposits in patients with AL amyloidosis. *Blood.* 2010;116:2241–2244.
13. Klunk WE, Engler H, Nordberg A, et al. Imaging brain amyloid in Alzheimer's disease with Pittsburgh Compound-B. *Ann Neurol.* 2004;55:306–319.
14. Gertz MA, Comenzo R, Falk RH, et al. Definition of organ involvement and treatment response in immunoglobulin light chain amyloidosis (AL): a consensus opinion from the 10th International Symposium on Amyloid and Amyloidosis, Tours, France, 18-22 April 2004. *Am J Hematol.* 2005;79:319–328.
15. Ihse E, Suhr OB, Hellman U, Westermark P. Variation in amount of wild-type transthyretin in different fibril and tissue types in ATTR amyloidosis. *J Mol Med (Berl).* 2011;89:171–180.
16. Westermark GT, Sletten K, Westermark P. Alkali-degradation of amyloid: an ancient method useful for making monoclonal antibodies against amyloid fibril proteins. *Scand J Immunol.* 2009;70:535–540.
17. Westermark P, Davey E, Lindbom K, Enqvist S. Subcutaneous fat tissue for diagnosis and studies of systemic amyloidosis. *Acta Histochem.* 2006;108:209–213.
18. Buck A, Wolpers HG, Hutchins GD, et al. Effect of carbon-11-acetate recirculation on estimates of myocardial oxygen consumption by PET. *J Nucl Med.* 1991;32:1950–1957.
19. Timmer SA, Lubberink M, Germans T, et al. Potential of [^{11}C]acetate for measuring myocardial blood flow: Studies in normal subjects and patients with hypertrophic cardiomyopathy. *J Nucl Cardiol.* 2010;17:264–275.
20. van den Hoff J, Burchert W, Borner AR, et al. [1-^{11}C]acetate as a quantitative perfusion tracer in myocardial PET. *J Nucl Med.* 2001;42:1174–1182.
21. Watabe H, Jino H, Kawachi N, et al. Parametric imaging of myocardial blood flow with ^{15}O-water and PET using the basis function method. *J Nucl Med.* 2005;46:1219–1224.
22. Harms HJ, Knaapen P, de Haan S, Halbmeijer R, Lammertsma AA, Lubberink M. Automatic generation of absolute myocardial blood flow images using [^{15}O]H_2O and a clinical PET/CT scanner. *Eur J Nucl Med Mol Imaging.* 2011;38:930–939.
23. Boellaard R, Knaapen P, Rijbroek A, Luurtsema GJ, Lammertsma AA. Evaluation of basis function and linear least squares methods for generating parametric blood flow images using ^{15}O-water and positron emission tomography. *Mol Imaging Biol.* 2005;7:273–285.
24. Cerqueira MD, Weissman NJ, Dilsizian V, et al. Standardized myocardial segmentation and nomenclature for tomographic imaging of the heart: a statement for healthcare professionals from the Cardiac Imaging Committee of the Council on Clinical Cardiology of the American Heart Association. *Int J Cardiovasc Imaging.* 2002;18:539–542.
25. Cornwell GG 3rd, Murdoch WL, Kyle RA, Westermark P, Pitkanen P. Frequency and distribution of senile cardiovascular amyloid. A clinicopathologic correlation. *Am J Med.* 1983;75:618–623.
26. Harms H, de Haan S, Knaapen P, et al. Tracer kinetic analysis of myocardial [^{11}C]hydroxyephedrine studies [abstract]. *J Nucl Med.* 2011;52(suppl 1):254.
27. Iida H, Kanno I, Takahashi A, et al. Measurement of absolute myocardial blood flow with $H_2{}^{15}O$ and dynamic positron-emission tomography: strategy for quantification in relation to the partial-volume effect. *Circulation.* 1988;78:104–115.
28. Tsai SB, Seldin DC, Wu H, O'Hara C, Ruberg FL, Sanchorawala V. Myocardial infarction with "clean coronaries" caused by amyloid light-chain AL amyloidosis: a case report and literature review. *Amyloid.* 2011;18:160–164.